Research Square

Preprints are preliminary reports that have not undergone peer review.
They should not be considered conclusive, used to inform clinical practice,
or referenced by the media as validated information.

High Performance Epoxy Nanocomposite Linings for Underground Fuel Storage Tanks: Barrier Enhancement and Corrosion Protection

Buthaina S. Aziz

botheana.aziz@stu.edu.iq

Basra Engineering Technical College, Southern Technical University

Hisham Anwer Salih

University of Basrah

Dalal N. Alhilfi

University of Basrah

Abdullah. A. Hussein

University of Basrah

Research Article

Keywords: Epoxy coatings, Underground storage tanks, Nanocomposite coatings, Corrosion protection, Chloride environment

Posted Date: June 24th, 2026

DOI: https://doi.org/10.21203/rs.3.rs-10029273/v1

License: This work is licensed under a Creative Commons Attribution 4.0 International License.
Read Full License

Additional Declarations: No competing interests reported.

High Performance Epoxy Nanocomposite Linings for Underground Fuel Storage Tanks: Barrier Enhancement and Corrosion Protection

Buthaina S. Aziz [1], Hisham Anwer Salih[2], Dalal N. Alhilfi [3], Abdullah. A. Hussein [3]

[1]Chemical and Petrochemical Engineering Department, Basra Engineering Technical College, Southern Technical University, Basra, Iraq.
[2]University of Mosul, College of Education for pure science, Department of physics
[3]Polymer Research Centre, University of Basrah, Basrah, Iraq.

Abstract

Epoxy (EP) coatings are widely applied for corrosion protection; however, their barrier performance may deteriorate in chloride environments due to electrolyte uptake and degradation at the coating-metal interface. In this study, metal vanadium oxyphosphate nanofillers (M-VP; M = Co, Zn, and Mg; VP = $VOPO_4$) were synthesized and incorporated into a Bisphenol-F epoxy at a fixed loading of 1 wt%, producing coatings with a controlled dry-film thickness of ~40 µm. SEM was used to examine surface morphology, and barrier properties were evaluated using electrochemical impedance spectroscopy after 30 days of immersion in 3.5 wt% NaCl. All nanocomposite coatings exhibited enhanced barrier performance compared with neat epoxy, with the anticorrosion efficiency following the order EP < EP-CoVP < EP-ZnVP < EP-MgVP. Water absorption was markedly suppressed in the Mg-containing system, decreasing to 0.8% compared with 13% for EP, while the disbonded area was reduced from 18 to 1.5 mm^2. Mechanical and surface properties were also improved, with impact resistance increasing from 6.67 to 9.32 J and the water contact angle rising from 60° to 90°. Overall, Mg-VP proved to be the most effective nanofiller for improving the durability of epoxy coatings in chloride environments.

Graphical Abstract:



Keywords: Epoxy coatings; Underground storage tanks; Nanocomposite coatings; Corrosion protection; Chloride environment.

1 .Introduction

Underground storage tanks (USTs) are an essential part of energy and water infrastructure and are designed to hold large volumes of liquid and gaseous materials. Leakage poses a severe threat to the environment, human health, and the economy by polluting soil and groundwater. (Guignet and Martinez-Cruz, 2018; Kouser *et al.*, 2025). Therefore, protective linings are essential. Thermosetting polymers, such as epoxy resins, are promising candidates for this role, as they have a strong reputation for structural and insulating performance. (Muresan, 2023; Zaghloul, Zaghloul and Fuseini, 2023)

These materials are applied to exterior and interior surfaces, or as lining, on concrete and metal tanks, creating an unbroken, impervious coating. (Ramakrishnan *et al.*, 2022; Xavier, 2022). Epoxy's mechanical properties are relatively stable, allowing it to be used in demanding construction applications. High binding power is emphasized, as it indicates strong attachment to concrete and steel surfaces; hence, the insulating layer will remain sticky under various operating conditions. (Radhamani, Lau and Ramakrishna, 2020; Zhu *et al.*, 2024). The cross-cut test is usually used to measure this performance. (Kausar, 2020)

Formulations based on nanomaterials are also superior at retaining this adhesion under stress. (Fang, Guo and Si, 2021). Durability-wise, it is impact-resistant and rigid, so that it can withstand scratches or accidental shocks during maintenance or in its environment. (Figueira, Silva and Pereira, 2015). Although epoxy is traditionally deemed tough, it can be made to have a certain amount of tolerable flexibility by using the right curing agent (e.g., cycloaliphatic agents) so that it can pass the bending test and resist vibration or other small deformations in the tank structure without cracking, which is also verified by measurements of elasticity by Dynamic Mechanical Analysis (DMA) (Zhao *et al.*, 2021; Amin *et al.*, 2022).

The chemical properties of epoxy are sufficient to consider it the pillar of its effectiveness as a sealant barrier. It creates an almost waterproof, moisture-proof layer that excludes one of the most significant causes of tank damage and leakage. (Bratasyuk, Latyshev and Zuev, 2023). This is demonstrated by the extremely low water absorption of the optimized formulations. (Pan *et al.*, 2026). It is also a chemical-resistant compound to a wide range of agents, including acids, alkalis, organic solvents, and petroleum derivatives, as samples do not change when placed in these liquids, particularly in formulations prepared with modified cycloaliphatic agents. (Sasaki, 2007; Luo *et al.*, 2023)

Epoxy is also demonstrating its efficacy in steel tank protection, as an epoxy-based coating containing vanadium phosphate nano-additives has excelled in electrochemical impedance spectroscopy (EIS) and salt spray tests and offers high polarity resistance. Notably, permeability tests in the future use of

epoxy in storing gas in disused mines, as hydrogen has demonstrated that the material can provide a sound barrier against leakage of small particles, and its liquid form before solidifying can permeate and seal the tiniest cracks in the current concrete structures, and seal the structure completely, and offer added protection.(Deyab *et al.*, 2021, 2024; Gajda, 2021; Liu *et al.*, 2024)

Although widely applied, the relative roles of $VOPO_4$-type nanofillers (Co, Zn, Mg) on epoxy barrier life under the same preparation and exposure conditions have not yet been adequately determined. This work is novel in two aspects: (i) It offers the head to head comparison of Co-, Zn-, and Mg-$VOPO_4$) (nanofillers at the same loading (1 wt%) into the same epoxy system and applied at controlled thickness, eliminating the formulation and geometry bias; (ii) It goes beyond the qualitative discussion to extract and compare physically meaningful EIS-derived parameters (e.g., coating/pore resistance, interfacial charge transfer resistance, and coating capacitance/water-absorption indicators) after 30 days immersion.

2. Materials and Methods

The polymer matrix was epoxy resin Bisphenol-F (Bisphenol F diglycidyl ether (BPF-DGE), Epoxy Equivalent Weight (EEW)= 160–175 $g \cdot eq^{-1}$, density=1.2 g/cm^3, and viscosity =1200 mPa·s). The curing agent was a commercial cycloaliphatic hardener, and the diluent was xylene. All chemicals used were analytical or commercial grade and were used without further processing, unless otherwise noted. All aqueous preparations were done using deionized water. The precursors of M-VP were ammonium metavanadate (NH_4VO_3), acetic acid (CH_3COOH), hydrated metal nitrates [$M(NO_3)_2.6H_2O$; M = Co, Zn, Mg], and ammonium phosphate ($NH_4H_2PO_4$) (Brasher and Kingsbury, 1954)

2.2 Synthesis of metal vanadium oxyphosphate nanofillers

M-VP nanofillers were prepared via solvothermal synthesis. In a short time, NH_4VO_3 was dissolved in acetic acid (1:1) in distilled water to yield a clear solution (Solution A). To Solution A, the equivalent metal nitrate salt [$M(NO_3)_2 \cdot 6H_2O$] was added, stirred until dissolved, and heated to high temperature to homogenize. At the same time, solution B ($NH_4H_2PO_4$ aqueous) was prepared and dropwise added to solution A in constant stirring to maintain the precipitation and uniformity of the nucleation. The resulting mixture was placed in a Teflon-lined autoclave and subjected to solvothermal conditions. The resulting solids were filtered, rinsed several times with deionized water to remove soluble by-products, and dried under vacuum before use as fillers (Amedzo-Adore and Han, 2022). All metal systems had the same synthesis parameters (autoclave configuration, solvent composition, initial pH, reaction temperature, and time), and post-treatment conditions were kept

constant to ensure phase comparability and to remove synthesis-related bias in later characterization and coating performance analysis. Table 1 summarizes the conditions of the fixed synthesis. The solids were collected after natural cooling to room temperature, washed with large volumes of deionized water until a pure, neutral filtrate was obtained, and dried under vacuum at 70 °C for 3 hr.

Table 1. Solvothermal Synthesis conditions for M-VP nanofillers (M = Co, Zn, Mg and $VOPO_4$)

Parameter	Value
Autoclave type	Teflon-lined stainless steel
Autoclave nominal volume	100 mL
Solvent system	DI water : acetic acid = 1:1 (v/v)
Initial pH (before sealing)	2.8-3.2
Reaction temperature	160 °C
Reaction time	12 h
Stirring before autoclaving	600 rpm, 50 min
Cooling after reaction	Natural cooling to room temperature
Washing	DI water
Drying	Vacuum drying at 70 °C for 3 h

2.3 Epoxy nanocomposite coating formulations preparation

Upon addition of 1 wt% of M-VP nanofillers (Co-VP, Zn-VP, Mg-VP) to the epoxy system, three epoxy nanocomposite formulations were prepared and labeled EP-MgVP, EP-CoVP, and EP-ZnVP, respectively. Filled epoxy and EP (without filler) were prepared as references. The use of metal vanadium oxyphosphate (VP-type) nano-additives in epoxy coatings has already been investigated as a corrosion-protection additive. Thus, it can be considered a functional barrier filler in the current formulations. (Honarvar Nazari *et al.*, 2022).

2.4. Preparation of substrate and coating of substrate.

A coating was applied to carbon steel coupons, which served as substrates and as electrochemical testing working electrodes. Before coating, the surfaces were treated according to a standard cleaning procedure outlined in ASTM G1-03. (ASTM, 2003; Standard, 2003), including removal of corrosion

products, degreasing with a suitable solvent, rinsing with deionized water, and drying. The coatings were then applied immediately after surface preparation with a film applicator, ensuring uniform films and reducing thickness gradients. In the electrochemical test, the test area was exposed and controlled to avoid edge effects and crevice contributions during immersion. Coated panels were left to cure under controlled conditions until fully cured, then stored in a clean, dry environment until testing.

2.5 Coating thickness control

Dry film thickness (DFT) was measured with a micrometer and kept constant (~40 µm) across all samples. Thickness was maintained across all formulations to remove the thickness-dependent bias in the impedance response and to ensure that the effects of nanofiller incorporation are the primary mechanism underlying the observed differences in barrier properties, rather than geometric effects. (International, 2021)The figure below provides a schematic overview of the key steps in preparing an epoxy nanocomposite coating.



Figure 1. The flowchart illustrates the main steps involved in preparing VP-based epoxy nanocomposite coatings.

The epoxy resin was mixed with the fillers (1 wt%) by mechanical stirring at 1000 rpm for 30 min, followed by ultrasonic dispersion for 10 min. The curing agent was then added at a 2:1 resin-to-hardener ratio, and the mixture was applied to steel substrates. The coating was dried at room temperature (24 h) and post-dried at 60 ^{o}C for 4 h.

2.6 Scanning Electron Microscopy (SEM)

The scanning electron microscopy (SEM) was used to study the surface morphology of the epoxy nanocomposite coating. An InLens detector was used for SEM at an accelerating voltage of 10.0 kV and a working distance of 6.4 mm. The micrographs were captured at a magnification of about 10,2000x. The coating samples were prepared correctly, and the images were acquired under high-vacuum conditions before SEM examination. The micrograph includes a 10 µm scale bar. To

qualitatively determine the homogeneity of the surface, the density of defects, and the overall morphological characteristics of the coatings.

2.7 Electrochemical impedance spectroscopy (EIS)

EIS measurements were performed in a standard three-electrode cell with a coated steel specimen as the working electrode, a saturated calomel electrode (SCE) as the reference electrode, and a platinum counter electrode. The aqueous sodium chloride solution (3.5 wt% NaCl) was used as the electrolyte. Electrochemical impedance spectroscopy (EIS) measurements were carried out using a small-amplitude sinusoidal perturbation (10 mV) over a broad frequency range (0.01 Hz to 100 kHz). Before the impedance measurements were taken, coated samples were pre-exposed (30 days) to the electrolyte to test the stability of the barriers under extended exposure to chloride. The temperature was regulated during measurements using a thermostatic bath. This is a non-destructive quantitative evaluation of coating condition and deterioration due to electrolyte penetration, demonstrating coating quality and barrier efficacy. (Thitsartarn and Jinkarn, 2021)

$$\Phi w = \left[\frac{log\,(^{Ct}/_{C_\circ})}{log\,(\varepsilon_w)}\right] \times 100\% \qquad 1$$

Where: Φ_w: Water absorption of the coating expressed as a percentage, Ct: Coating capacitance measured after an immersion time t, obtained from EIS fitting, C_0: Initial coating capacitance measured at t = 0, and ε_w: Relative dielectric constant of water (Taken as 80 at 25 ^oC).

Figure 2 demonstrates that electrochemical impedance spectroscopy (EIS) data were analyzed by equivalent electrical circuit (EEC) models. (a) The circuit includes the solution resistance (Rs), coating capacitance (Cc), pore resistance (Rpo), and the interfacial components of the double-layer capacitance (Cdl) and charge-transfer resistance (Rct), which characterize charge-transfer reactions at the steel/coating interface. When the coating's barrier behavior controlled the impedance behavior, the simplified circuit in (b), comprising (Rs), (Cc), and (Rpo), was applied. The EIS spectra were compared with the chosen circuit to obtain values (Rpo) and (Rct) to compare the performance of the coating barrier and corrosion protection (Bravo-Yumi *et al.*, 2020; OYELAMI. *et al.*, 2025)

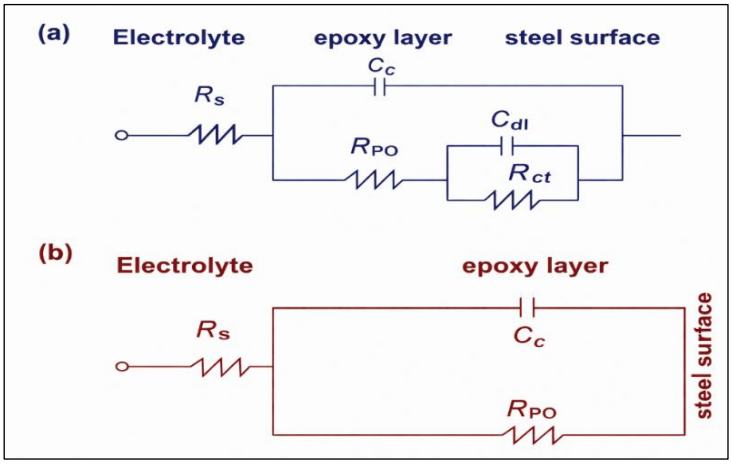


Figure 2. Electrical circuit models of the EIS response of epoxy-coated steel: (a) circuit with coating and charge transfer processes at the steel-coating interface, (b) simplified circuit with the barrier behavior of the epoxy coating.

A change in dielectric properties upon immersion was used to measure coating water absorption behavior, with coating capacitive parameters serving as indicators of dielectric changes extracted from EIS fitting. The comparative coating shift capacitance was connected with water absorption through a commonly known capacitance-water absorption method in the literature. The assumptions and parameter definitions (initial capacitance at time zero vs. capacitance after immersion) were used uniformly across all formulations to allow ranking. (OYELAMI *et al.*, 2025).

2.8 Thermal and mechanical characterization

DSC was used to study thermal behavior to assess the glass transition, and DMA was used to investigate viscoelastic response as an indicator of network stability. Mechanical/physical screening consisted of cross-cut adhesion, impact strength, bending flex, and contact angle to assess surface wettability and potential decreases in electrolyte affinity. Testing was carried out across all formulations, and successive measurements were performed on a separate, independently prepared sample to verify reproducibility. (ISO, 2019)

3. Results and Discussion

3.1. Structural confirmation of VP nanofillers

Figure 3 (a-d) demonstrates the X-ray diffraction (XRD) patterns of the prepared (a) EP, (b) Mg-VP, (c) Co-VP, and (d) Zn-VP nanofillers. The X-ray diffraction pattern of epoxy (EP) is presented in (a). The trend shows a wide, diffuse halo centered at 18-25°, which is typical of amorphous, cured epoxy. No sharp diffraction peaks are observed, indicating that epoxy lacks long-range crystalline order and

therefore has mostly a non-crystalline (amorphous) structure. The diffraction patterns of all samples show a sequence of sharp, distinct peaks, indicating that the prepared vanadium phosphate compounds are crystalline. The diffraction pattern of EP-ZnVP, as shown in (b), demonstrates strong reflections at the angles of 18.9, 21, 24.9, 27.1, 29.3, 31.7, 34.9, 37.8, and 43.6 °, which validates the crystal structure of EP-ZnVP. The XRD profile of EP-CoVP (c) has the same diffraction characteristics as the major peaks at approximately 19.0, 21.3, 25.2, 27.4, 29.6, 32.0, 35.1, and 40.3 °. Changes in the positions of the peaks in connection with Mg-VP may be explained by changes in the ionic radii and distortion of the lattice experienced by the addition of the Co-VP structure. In (d), the observed diffraction peaks of EP-MgVP at 18.6, 20.1, 24.7, 26.8, 28.9, 31.2, 34.6, and 38.9 ° could be attributed to the crystal planes of the monoclinic vanadium phosphate phase, characteristic of the structure, and indicate that it was successfully formed. The names of these peaks are high and narrow, implying a high degree of crystallinity and even crystal growth.

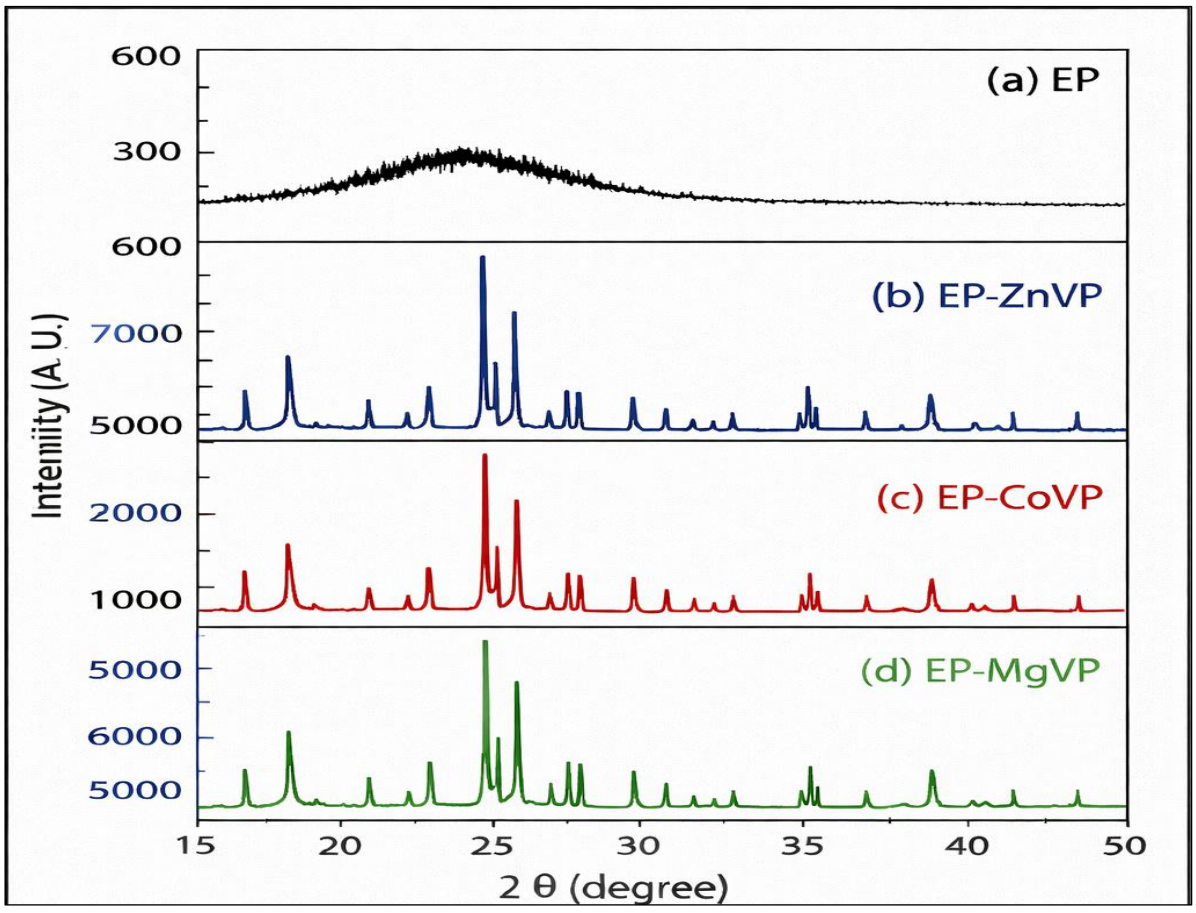


Figure 3. XRD patterns of synthesized (a) EP, (b) Mg-VP, (c) Co-VP, (d) Zn-VP, and (e) EP-MgVP nanofillers.

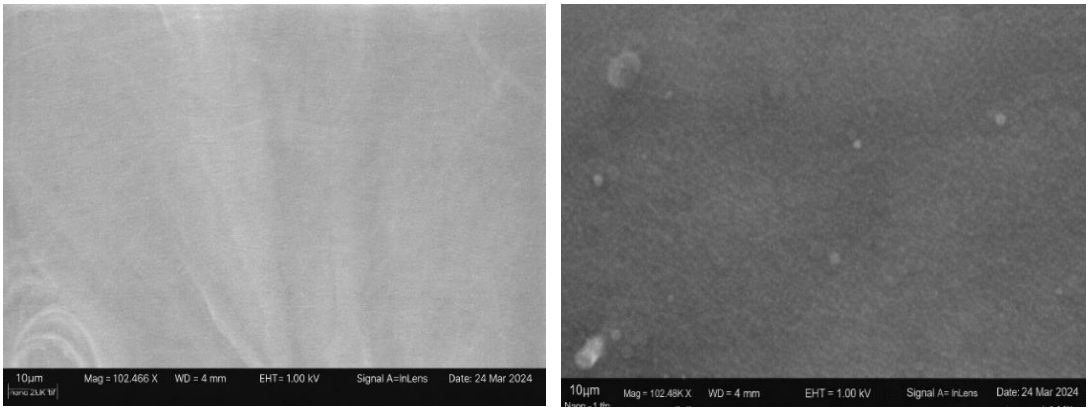
The presence of other high-angle peaks indicates a more ordered structure and perhaps stronger bonding between the metals and oxygen in the lattice. The absence of secondary or impurity peaks in

all samples suggests that the nanofillers are of pure phase. The minor differences in the peak intensity and position of Ep-Mg, Co, and ZnVP are associated with the different metal cations, which affect the lattice parameters, crystallinity, and defect density. These structural variations are believed to be important in regulating the distribution of nanofillers in the epoxy matrix and in their capacity to block microvoids and diffusion channels when applied to an epoxy coating.

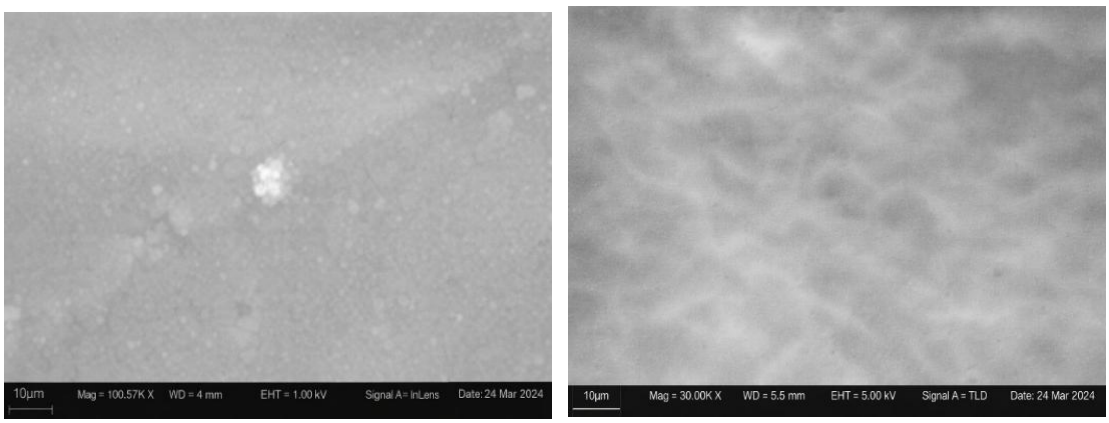
3.2 SEM Microstructural Analysis

Figure 4 shows that the surface morphologies align with the trends observed in the thermal, mechanical, and electrochemical measurements. The surface of EP coating (a) is homogeneous and relatively smooth, which is characteristic of a pure crosslinked structure with few particulate features. Following the addition of specific metal fillers, such as VP fillers, more and more surface textures are observed, indicating the presence and arrangement of inorganic phases within the polymer structure. The EP-CoVP (b) sample has the strongest surface roughness and visible clustered domains, suggesting partial agglomeration of filler particles. Such morphological heterogeneity is consistent with the increased Shore D hardness of the Co-containing coating, where rigid agglomerates can locally increase the matrix strength but, in addition, give rise to micro-interfaces that may not optimize barrier uniformity.

On the contrary, the morphology of the EP-ZnVP coating (c) is more balanced, and less harsh cluster structures are present, and the distribution is relatively even, which correlates with an intermediate position in the overall property rating. It is worth noting that the EP-MgVP (d) coating appears more compact and continuous, with fewer visible micro-pores and a denser surface texture. This small structure provides a probable microstructural explanation for its high-barrier performance (EIS), reduced water diffusion, and high contact angle, because a more dispersed/compact filler network may increase the diffusion tortuosity and decrease interlinking pathways for electrolyte and water transport.



(a) (b)



(c) (d)

Figure 4. SEM micrographs of epoxy coatings: (a) EP, (b) EP-CoVP, (c) EP-ZnVP, and (d) EP-MgVP.

3.3 Thermal transition behavior of epoxy nanocomposites (DSC)

Differential scanning calorimetry was used to analyze the thermal characteristics of EP- and VP-modified epoxy coating layers. A significant shift in the glass transition temperature (Tg) is observed in all nanocomposite systems, with Tg values higher than in EP, as indicated in Figure 5. The size of such a change is as follows:

EP-MgVP (105.2 ^{o}C) > EP-ZnVP (101.6 ^{o}C) > EP- CoVP (99.8 ^{0}C) > EP (96.3 ^{o}C)

The rise in Tg may be attributed to reduced polymer chain mobility induced by VP nanoparticles. Self-assembly at the interphase between the filler surface restrains the segmental motion of the epoxy chains and decreases free volume, thereby improving thermal stability. This is the most significant effect on Mg-VP, indicating stronger interfacial interactions or greater dispersion in the epoxy matrix. The increased Tg is beneficial for underground storage tank linings because it reduces the risk of softening, cracking, and early degradation caused by thermal effects during extended service.

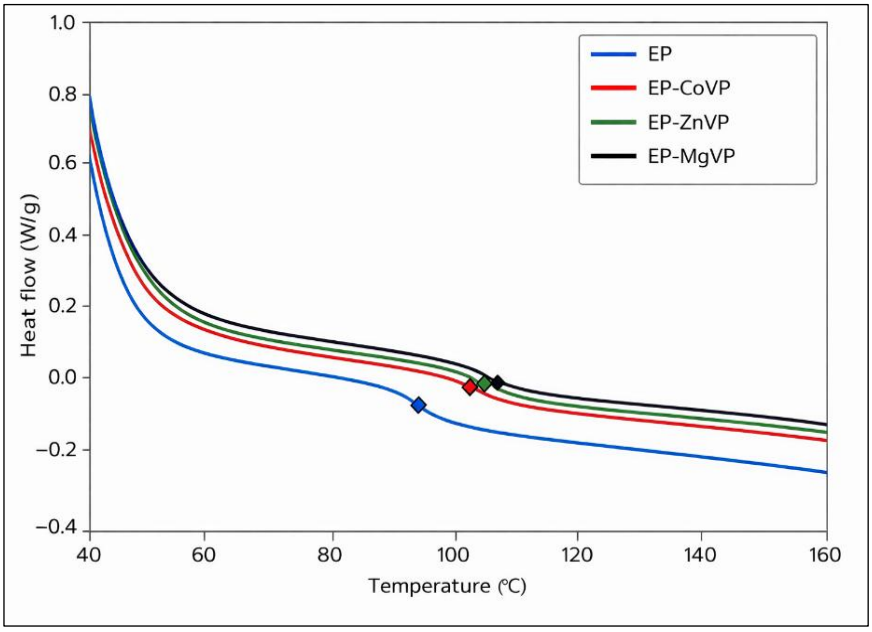


Figure 5. DSC thermograms of EP and VP-based epoxy nanocomposites (EP-CoVP, EP-ZnVP, and EP-MgVP).

Incorporating M-VP nanofillers significantly increases the impact strength and surface wettability of epoxy compared with pure resin. The EP has the lowest impact resistance (6.67 J) and contact angle (60), while the nanocomposites have higher impact resistance (8.44-9.32 J) and contact angles (87-90). An improvement in impact performance is due to the reinforcing effect of the nanofillers, which facilitate stress transfer and prevent crack initiation/propagation. The increased contact angles indicate lower water affinity, which can restrict water absorption and delay electrolyte intrusion. EP-MgVP is the most successful formulation (9.32 J, 90 degrees), as expected, due to stronger filler/matrix interactions and greater improvement in properties (Table 2).

Table 2. Impact resistance and water contact angle of EP and metal phosphate-modified epoxy composites.

Sample	Impact Resistance (J)	Contact Angle (°)
EP	6.67	60
EP-CoVP	8.44	87
EP-ZnVP	8.73	88
EP-MgVP	9.32	90

3.4. Electrochemical impedance response and barrier performance

Figure 6 shows the electrochemical impedance spectroscopy results, obtained to determine the corrosion-barrier performance of the coatings after 30 days of immersion in a 3.5 wt% NaCl solution. Nyquist plots show that the VP-modified epoxy coating exhibits a much larger capacitive arc than EP, which has lower impedance and poorer barrier behavior. The capacitive arc diameter of the nanocomposites is related in the order: EP-MgVP, EP-ZnVP, EP-CoVP, and EP. This tendency indicates increased resistance to electrolyte penetration and a slowed onset of interfacial electrochemical processes. This process is regulated by a tortuous path in which dispersed VP nanoparticles block microvoids in the epoxy matrix, and corrosive species diffuse along longer, less-connected pathways. Consequently, ionic transfer and charge transfer between the metal/coating interface are inhibited.

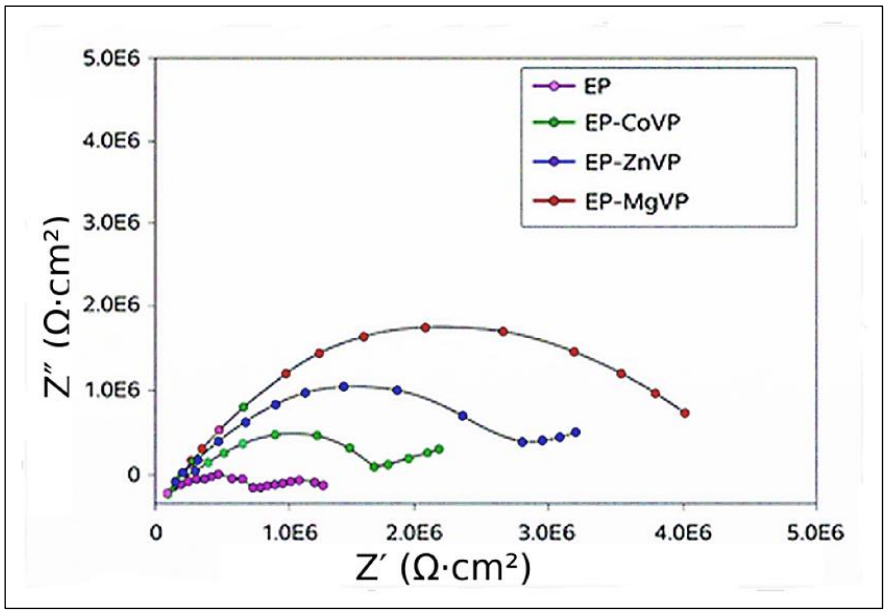


Figure 6**.** Nyquist plots of EP- and VP-modified epoxy coatings after immersion in 3.5 wt% NaCl, showing an enhanced impedance response for the nanocomposite coatings.

3.5 Equivalent circuit parameters and water absorption implications

To quantify the EIS response, the impedance spectra were modelled using the equivalent circuit models outlined in the experimental section. The parameters obtained indicate that incorporating VP results in a significant increase in the coating resistance (Rpo) and the interfacial charge-transfer resistance (Rct), and a decrease in the effective coating capacitance, as shown in Figure 7. Coating capacitance is strongly affected by water absorption because water has a high dielectric constant; thus, a decrease in capacitance indicates reduced electrolyte absorption and lower effective porosity.

This is most pronounced in the EP-MgVP system and demonstrates the typical high-resistance, low-capacitance characteristic associated with high levels of barrier integrity.

These findings validate the idea that VP nanofillers can not only slow ionic diffusion but also reduce dielectric variations associated with water intrusion, indicating the coating's durability over 30 days. For the P-Mg/epoxy composite, the EIS spectrum was likely controlled by the coating. It did not show a clear low-frequency interfacial charge-transfer characteristic, so no reliable Rct/Cdl pair could be fitted. The extremely large Rpo indicates a high level of barrier performance, inhibiting electrolyte access and rendering charge transfer insignificant over the measured frequency range; therefore, Rct and Cdl could not be physically separated.

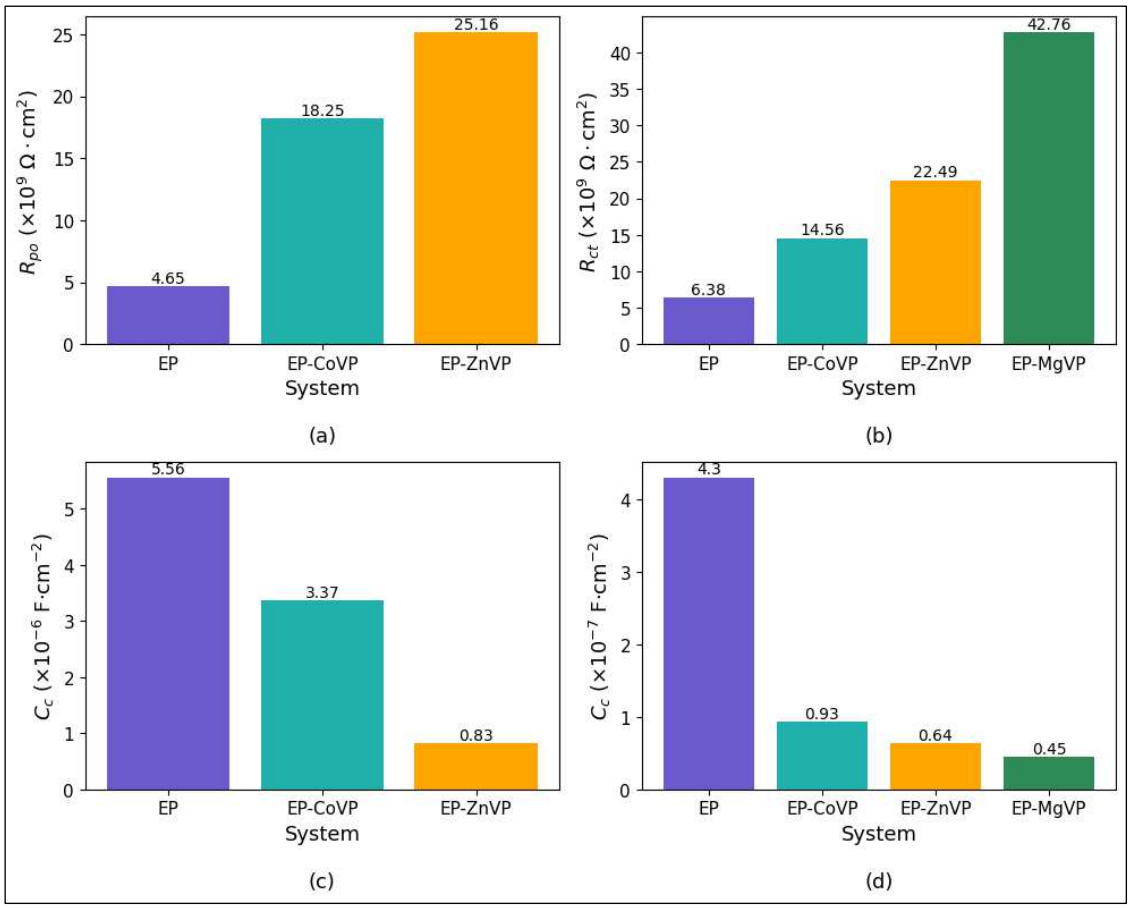


Figure 7**.** Schematic representation of EIS-derived trends for EP and VP-based nanocomposites: (a) coating resistance (Rpo), (b) charge transfer resistance (Rct), and (c) coating capacitance.

3.6 Interfacial stability and degradation based on adhesion

The interfacial degradation of epoxy coatings is closely related to water absorption. Table 3 shows that EP exhibits the highest water absorption (13%) and the largest disbonded area (18 mm2), indicating susceptibility to electrolyte ingress and film degradation. Introduction of VP nanofillers

significantly reduces water absorption and the area of disbonding, indicating improved barrier continuity and a more stable interface. EP-MgVP has the lowest water absorption (0.8%) and the smallest disbonded area (1.5 mm2), which aligns with its best barrier properties as seen in EIS.

Table 3. Disbonded area and water absorption for EP and VP-based epoxy nanocomposite coatings after immersion.

Sample	Disbonded area (mm^2)	Water absorption (%)
EP	18	13
EP-CoVP composite	17	5.5
EP-ZnVP composite	3	2.5
EP-MgVP composite	1.5	0.8

3.7 Thermal effect on shore D hardness of pure and M-filled epoxy

Figure 8 demonstrates how Shore D hardness depends on temperature in EP and epoxy nanocomposites strengthened with M-VP (M= Co, Zn, and Mg). In all systems, a gradual decline in hardness is observed as temperature increases, accompanied by softening of the epoxy matrix. With increased temperature, the resistance to indentation decreases due to increased segmental mobility of the polymer chains, and consequently, the Shore D values decrease. Although this is the overall trend, the nanocomposite coatings consistently have higher hardness than the EP at all temperatures studied.

This tendency suggests that the inorganic nanofillers exert a reinforcing effect and limit polymer chain motion through strong interfacial interactions and enhanced load transfer within the epoxy network. This is because rigid M-VP particles act as a physical barrier to deformation, thereby retarding the initiation of thermal softening. The EP-CoVP system is the hardest of the nanocomposites at all temperatures, followed by EP-ZnVP and EP-MgVP. This ranking implies that filler-matrix interactions and dispersion efficiency differ, and both determine the level of chain immobilization and the thermal stability of the composite structure. The difference in hardness between EP and the nanocomposites is more pronounced at higher temperatures (≥80 °C), underscoring the enhanced thermal resistance of the reinforced systems.

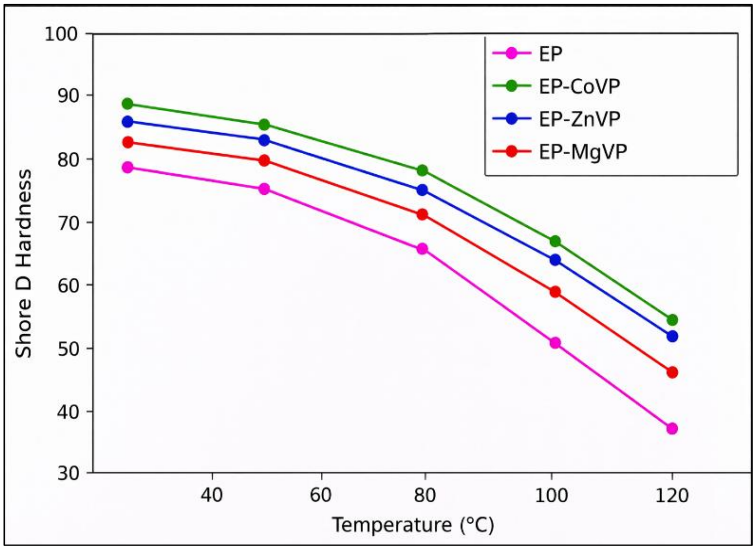


Figure 8. Temperature dependence of Shore D hardness for EP and EP-CoVP, EP-ZnVP, and EP-MgVP composites.

3.8 The effect of the Metallic reinforcement on the mechanical properties

Figure 9 (a-d), a comparison of the mechanical response of the epoxy-based systems is made. Metallic reinforcements enhance overall load-bearing capacity compared to EP, as indicated by increases in compressive and tensile strength, and the Ep-CoVP composite exhibits the best strength levels. This reinforcement is accompanied by an increase in Young's modulus, indicating that the material becomes more rigid. This may be explained by its ability to transfer stress more effectively and by its matrix being less deformable. Nevertheless, the reinforced systems exhibit lower break elongation than EP, indicating reduced ductility due to limited polymer chain mobility and the formation of particle-matrix interfaces that can create local stress concentrations. The variations in Mg-, Co-, and Zn-reinforced composites emphasize that mechanical performance is determined by the efficiency of the reinforcement-matrix interaction, with stiffness and strength versus ductility.

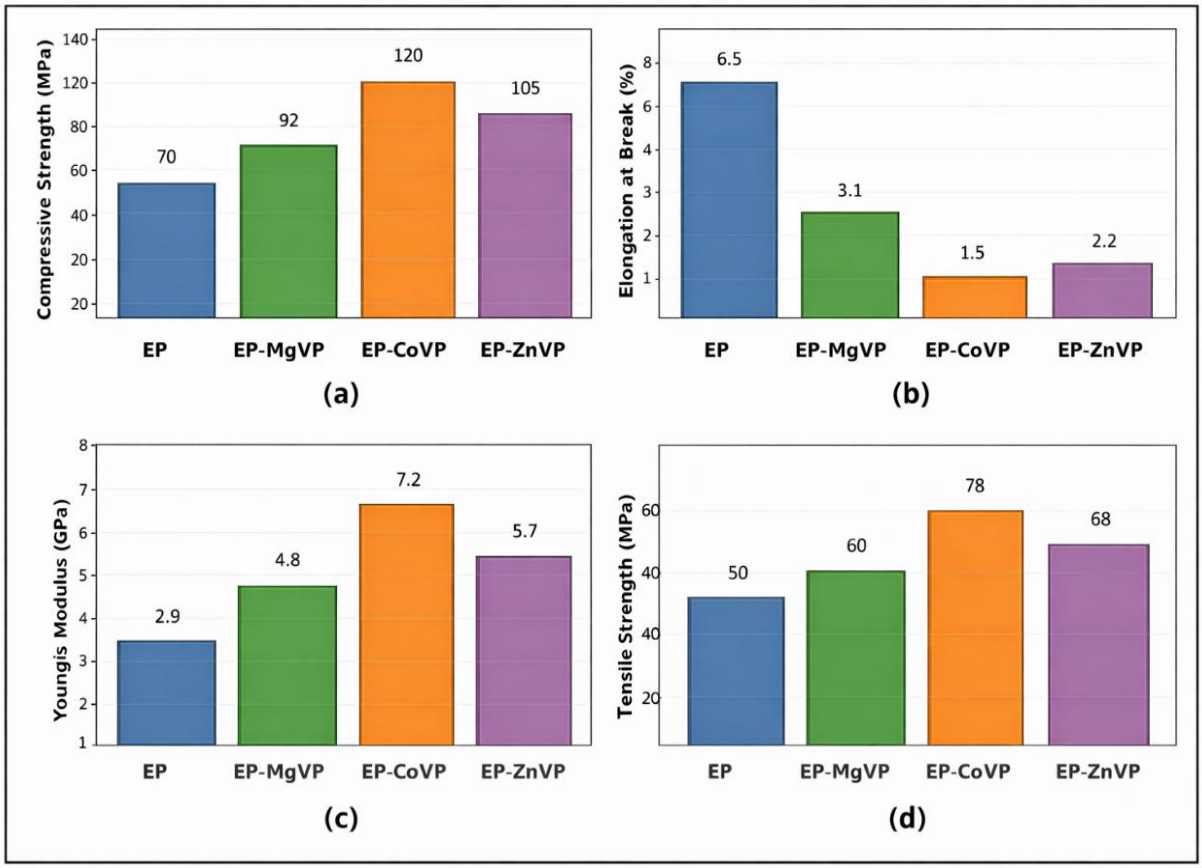


Figure 9. Comparative bar charts illustrate the mechanical properties of epoxy-based composites reinforced with different metals: (a) compressive strength, (b) elongation at break, (c) Young's modulus, and (d) tensile strength.

4. Conclusions

This study provides a systematic comparison of metal-modified vanadium phosphate fillers (M-VP, where M is Co, Zn, or Mg, and VP is VOPO4) in epoxy coatings at a low loading (1 wt%) to improve barrier properties and corrosion resistance. All M-VP coatings were found to outperform the pure epoxy system, and their protective efficiency was significantly enhanced at the expense of the nature of the incorporated metal ion. The EP-MgVP coating showed the smallest filler morphology and the most uniform distribution of the filler, indicating the best interfacial compatibility between the filler and the polymer matrix. These structural merits were directly translated into improved electrochemical performance. The results of electrochemical impedance spectroscopy (EIS) indicated that the Mg-VP-reinforced coating exhibited the highest resistance and the slowest deterioration during immersion, indicating effective inhibition of ionic transport and a delay in the formation of conducting pathways within the coating. Moreover, the modified coating had lower water absorption and greater mechanical integrity and chemical resistance than the EP system. In summary, the research findings reveal that maximizing filler chemistry and dispersion at

low loading rates is a highly effective approach for developing durable anticorrosion coatings on metallic substrates in harsh environments using an epoxy-based resin.

Acknowledgements

The authors would like to express their sincere appreciation to the Southern Technical University, Basrah, Iraq, Polymer Research Centre, and the Department of Chemical Engineering at the University of Basrah for providing the facilities and technical support required to carry out this work and for its cooperation during the experimental investigations.

Funding

This research did not receive any specific grant from funding agencies in the public, commercial, or non-profit sectors.

Declaration of generative AI use

During the preparation of this manuscript, the authors used AI-assisted language tools to improve the text's grammar, clarity, and readability. After using these tools, the authors critically reviewed, edited, and validated the content and took full responsibility for the accuracy, originality, and integrity of the published work.

References

Amedzo-Adore, M. and Han, J.I. (2022) 'Chemically lithiated layered VOPO4 by a microwave-assisted hydrothermal method and its electrochemical properties in rechargeable Li-ion batteries and supercapacitor applications', *Journal of Alloys and Compounds*, 911, p. 165067. Available at: https://doi.org/10.1016/j.jallcom.2022.165067.

Amin, K.F. *et al.* (2022) 'Polymer nanocomposites for adhesives and coatings', in *Advanced Polymer Nanocomposites*. Elsevier, pp. 235–265. Available at: https://doi.org/10.1016/B978-0-12-824492-0.00014-3.

ASTM, G. (2003) 'Standard practice for preparing, cleaning, and evaluating corrosion test specimens', in *American Society for Testing and Materials*.

Brasher, D.M. and Kingsbury, A.H. (1954) 'Electrical measurements in the study of immersed paint coatings on metal. I. Comparison between capacitance and gravimetric methods of estimating water-uptake', *Journal of Applied Chemistry*, 4(2), pp. 62–72. Available at: https://doi.org/10.1002/jctb.5010040202.

Bratasyuk, N.A., Latyshev, A. V. and Zuev, V. V. (2023) 'Water in Epoxy Coatings: Basic Principles of Interaction with Polymer Matrix and the Influence on Coating Life Cycle', *Coatings*, 14(1), p. 54. Available at: https://doi.org/10.3390/coatings14010054.

Bravo-Yumi, N. *et al.* (2020) 'Synthesis and characterization of Sb2O5-doped Ti/SnO2-IrO2 anodes toward efficient degradation tannery dyes by in situ generated oxidizing species', *Electrochimica Acta*, 358, p. 136904. Available at: https://doi.org/10.1016/j.electacta.2020.136904.

Deyab, M.A. *et al.* (2021) 'Design new epoxy nanocomposite coatings based on metal vanadium oxy-phosphate M0.5VOPO4 for anti-corrosion applications', *Scientific Reports*, 11(1), p. 8182. Available at: https://doi.org/10.1038/s41598-021-87567-3.

Deyab, M.A. *et al.* (2024) 'Impact of Co3O4 nanoparticles on epoxy's mechanical and corrosion-resistance properties for carbon steel in seawater', *Scientific Reports*, 14(1), p. 3535. Available at: https://doi.org/10.1038/s41598-024-53967-4.

Fang, T., Guo, R. and Si, Y. (2021) 'Ensemble Mode and Singular Value Based Road Texture-Skid Study', *Coatings*, 11(8), p. 947. Available at: https://doi.org/10.3390/coatings11080947.

Figueira, R.B., Silva, C.J.R. and Pereira, E. V. (2015) 'Hot-dip galvanized steel dip-coated with ureasilicate hybrid in simulated concrete pore solution: Assessment of coating morphology and corrosion protection efficiency', *Progress in Organic Coatings*, 88, pp. 245–255. Available at: https://doi.org/10.1016/j.porgcoat.2015.07.008.

Gajda, D. (2021) 'Epoxy Resin for Sealing the Underground Hydrogen Storage Reservoirs', in. Available at: https://doi.org/10.11159/ehst21.103.

Guignet, D.B. and Martinez-Cruz, A.L. (2018) 'The impacts of underground petroleum releases on a homeowner's decision to sell: A difference-in-differences approach', *Regional Science and Urban Economics*, 69, pp. 11–24. Available at: https://doi.org/10.1016/j.regsciurbeco.2017.12.006.

Honarvar Nazari, M. *et al.* (2022) 'Nanocomposite organic coatings for corrosion protection of metals: A review of recent advances', *Progress in Organic Coatings*, 162, p. 106573. Available at: https://doi.org/10.1016/j.porgcoat.2021.106573.

International, S. (2021) 'Practice for Nondestructive Measurement of Dry Film Thickness of Nonmagnetic Coatings Applied to Ferrous Metals and Nonmagnetic, Nonconductive Coatings Applied to Non-Ferrous Metals'. West Conshohocken, PA: ASTM International. Available at: https://doi.org/10.1520/D7091-21.

ISO, E.N. (2019) '2808; Paints and Varnishes—Determination of Film Thickness', *ISO: Geneva, Switzerland* [Preprint].

Kausar, A. (2020) 'Performance of corrosion protective epoxy blend-based nanocomposite coatings: a review', *Polymer-Plastics Technology and Materials*, 59(6), pp. 658–673. Available at: https://doi.org/10.1080/25740881.2019.1673410.

Kouser, T. *et al.* (2025) 'Applications of Epoxy Resins as a Coating Technology in Fluid Systems',

ChemBioEng Reviews, 12(2), p. e70000. Available at: https://doi.org/10.1002/cben.70000.

Liu, X. *et al.* (2024) 'Technical feasibility of converting abandoned calcite mines into lined rock caverns for underground hydrogen storage', *Journal of Energy Storage*, 86, p. 111051. Available at: https://doi.org/10.1016/j.est.2024.111051.

Luo, Y. *et al.* (2023) 'Enhanced adhesive and anti-corrosive performances of polymer composite coating for rusted metallic substrates by capillary filling', *Progress in Organic Coatings*, 178, p. 107467. Available at: https://doi.org/10.1016/j.porgcoat.2023.107467.

Muresan, L.M. (2023) 'Nanocomposite Coatings for Anti-Corrosion Properties of Metallic Substrates', *Materials*, 16(14), p. 5092. Available at: https://doi.org/10.3390/ma16145092.

OYELAMI., S. *et al.* (2025) 'CORROSION PROTECTION STRATEGIES FOR METALS USING NANOMATERIALS AND COATINGS', *Uniosun Journal of Engineering and Environmental Sciences*, 7(2). Available at: https://doi.org/10.64980/ujees.v7i2.446.

OYELAMI, S. *et al.* (2025) 'CORROSION PROTECTION STRATEGIES FOR METALS USING NANOMATERIALS AND COATINGS', *Uniosun Journal of Engineering and Environmental Sciences*, 7(2).

Pan, F. *et al.* (2026) 'Predicting, interpreting and optimizing water resistance in epoxy/amine coatings via machine learning and NSGA-II framework', *Corrosion Science*, 260, p. 113568. Available at: https://doi.org/10.1016/j.corsci.2025.113568.

Radhamani, A., Lau, H.C. and Ramakrishna, S. (2020) 'Nanocomposite coatings on steel for enhancing the corrosion resistance: A review', *Journal of Composite Materials*, 54(5), pp. 681–701. Available at: https://doi.org/10.1177/0021998319857807.

Ramakrishnan, T. *et al.* (2022) 'Study of Various Epoxy-Based Surface Coating Techniques for Anticorrosion Properties', *Advances in Materials Science and Engineering*. Edited by V. Vijayan, 2022(1), pp. 1–8. Available at: https://doi.org/10.1155/2022/5285919.

Sasaki, H. (2007) 'Curing properties of cycloaliphatic epoxy derivatives', *Progress in Organic Coatings*, 58(2–3), pp. 227–230. Available at: https://doi.org/10.1016/j.porgcoat.2006.09.030.

Standard, A. (2003) 'G1-03', *Standard Practice for preparing, cleaning, and evaluating corrosion test specimens, Annual Book of ASTM Standards*, 3, pp. 17–25.

Thitsartarn, W. and Jinkarn, T. (2021) 'Superhydrophobicity of paperboard packaging by hierarchical surface roughness modification of polylactic acid electrospraying', *Progress in Organic Coatings*, 154, p. 106192. Available at: https://doi.org/10.1016/j.porgcoat.2021.106192.

Xavier, J.R. (2022) 'Novel multilayer epoxy nanocomposite coatings for superior hydrophobic, mechanical and corrosion protection properties of steel', *Diamond and Related Materials*, 123, p. 108882. Available at:

https://doi.org/10.1016/j.diamond.2022.108882.

Zaghloul, Moustafa Mahmoud Yousry, Zaghloul, Mai Mahmoud Yousry and Fuseini, M. (2023) 'Recent progress in epoxy nanocomposites: corrosion, structural, flame retardancy and applications—a comprehensive review', *Polymers for Advanced Technologies*, 34(11), pp. 3438–3472.

Zhao, H. *et al.* (2021) 'The Curing Kinetics Analysis of Four Epoxy Resins Using a Diamine Terminated Polyether as Curing Agent', *Thermochimica Acta*, 702, p. 178987. Available at: https://doi.org/10.1016/j.tca.2021.178987.

Zhu, W. *et al.* (2024) 'Enhancing the corrosion resistance of waterborne epoxy coatings with functionalized biochar', *RSC Advances*, 14(53), pp. 39747–39758. Available at: https://doi.org/10.1039/D4RA07421A.